# Experimental Investigation and Optimization of AZ31 Mg Alloy during Warm Incremental Sheet Forming to Study Fracture and Forming Behaviour

Rohit Magdum [ORCID] and Pandivelan Chinnaiyan *

School of Mechanical and Building Sciences, VIT, Vellore 632014, India
* Correspondence: cpandivelan@vit.ac.in

**Abstract:** The main purpose of this research work is to study the forming limit and fracture behaviour of the AZ31 magnesium alloy, as well as to improve the formability and surface roughness of parts formed using the warm incremental sheet forming (ISF) process. For the ISF process, AZ31 Mg alloy sheets were used. Initially, Taguchi orthogonal L27 arrays were used to design experiments, and a framed multi-objective optimization problem was solved using the grey-fuzzy method. The strain-based forming fracture limit diagrams (FFLD) were plotted after a variable wall angle test. The grey-fuzzy reasoning grade (GFRG) is calculated in this study by combining grey relational analysis (GRA) and fuzzy rationale. For the AZ31 Mg alloy, the maximum GFRG value was obtained for the following forming combinations: step depth 0.3 mm, feed rate 500 mm/min, spindle speed 700 rpm, and tool diameter 10 mm. Then, ANOVA was used to determine the importance of parameters on the responses, and it was discovered that the step depth has the greatest influence (68.78%) on GFRG value, followed by the feed rate (16.56%). The fracture behaviour of the Mg alloy was studied using fractographs. Later, FE simulation was used to validate the strain value obtained from experimentation and to investigate the effect of process parameters on responses.

**Keywords:** magnesium alloy; incremental sheet forming; grey-fuzzy optimization; variable wall angle; warm forming; optimization

## 1. Introduction

For regular sheet metal forming, specialised equipment, such as dies and punches, and metal cutting and bending machines, are required to form the required part. As a result, the time and cost associated with the traditional sheet metal forming process are greater for customised products. Furthermore, any minor change in the part design may turn it into a herculean task because all of the requirements will be altered. Consumer demands are becoming more specific and personalised, rendering the traditional metal forming process obsolete. For these reasons, highly flexible forming methods with high dimensional precision are required. As a result, an additional efficient and adaptable forming process, namely incremental sheet metal forming (ISF), has evolved.

The ISF meets a unique set of requirements, including forming on standard CNC machines, die and punchless forming, low stress generation, rapid modification capability, higher material formability, and a superior surface finish at a low cost. Because of these characteristics, the ISF process is well suited for rapid prototyping in small- and medium-sized batch manufacturing [1]. Hence, determining the forming limit in the ISF process is very important. Pandivelan et al. [2] examined the formability of the sheet during the ISF process using a straight groove test and found that the formability was greatest in the rolling direction. Numerous researchers have investigated the strain-based forming limit for steel and its alloy sheets. Yoganjaneyulu et al. [3] observed that the formation of dimples, cracks, voids, and pits from a fractured surface disrupts the forming limit of

materials. According to this and other research, the strain-based forming limit of Mg alloys has not yet been determined and requires further investigation.

Magnesium is a lightweight material that is commonly used for biomedical implants and automobile components. The formability and surface quality of magnesium alloy when formed at higher temperatures are primarily influenced by several factors, such as the blank temperature during forming, type of lubricant, vertical step depth, sheet blank, and tool feed rate. Many researchers are interested in the anisotropy of Mg alloy sheets, which has a significant impact on the material formability and surface finish of the formed part [4].

Park et al. [5] emphasised the significance of magnesium alloy formation as mechanical properties improve. In another study, forming limit curves [6] at various temperatures were depicted as straight lines through the negative slopes, and the author concluded that grain size reduction increases the material's formability. Recently, Van and Nam [7] analysed the impact of tool vertical step depth and feed rate on the geometric accuracy and formability of AZ31 during warm incremental forming. Duflou et al. [8] implemented a laser beam to increase the formability of Al5182 material by warming the tool contact area and dimensional accuracy; the authors concluded that heating can extend formability. Attansaio et al. [9] modified the tool paths to improve the thickness uniformity, geometry precision, and surface quality. Using the ISF process, Ambrogio et al. [10] manufactured ankle supports with high precision.

Magnesium's hcp structure restricts dislocation movement/slip to basal planes, resulting in low formability and negligible ductility at room temperature. Therefore, Mg alloy sheets are formed at temperatures between 200 and 250 degrees Celsius. Park, J., et al., studied the effect of the tool radius, compared the obtained strain distribution to the forming limit curve (FLC), and accurately predicted the forming limit of magnesium alloy [5,11]. Ambrogio et al. concluded that at this temperature range, additional sliding planes are activated in addition to the basal plane, which significantly increases the formability of Mg alloy, with maximum formability occurring at 250 degrees Celsius [12].

Yasumasa et al. [13] investigated mechanical anisotropy caused by twinning in AZ31 Mg alloy and discovered that, as temperature increased, mechanical anisotropy decreased, resulting in the refinement of grains. Kleiner and Uggowitzer [14] also studied the deformation anisotropy of extruded Mg–Al–Zn magnesium alloy. Horng-Yu et al. [15] studied deformation characteristics for AZ61 thin alloy sheets influenced by temperature and mechanical anisotropy; in this work, the authors concluded that LZ61 alloy's drawability could be enhanced by an increase in average plastic strain ratio and a decrease in planer anisotropy with an increase in temperature. Zhang et al. [4] investigated the effect of anisotropy due to the sheet production method, i.e., different rolling directions of AZ31 Mg alloy sheets, and concluded that the anisotropy of the sheets significantly affects the surface quality of the resulting parts, and this effect decreases with increasing temperature.

Authors Pandey et al. [16] have applied the grey-fuzzy optimization strategy to the bone drilling procedure, and the results demonstrate the grey-fuzzy method's suitability for optimising multi-response characteristic problems. Biswajit et al. [17] have used the grey-fuzzy logic optimization technique to optimise CNC milling parameters, and they have concluded that the production of CNC milling is significantly increased with the aid of this technique.

The optimal process parameters for warm single point incremental forming (SPIF) of AZ31 magnesium alloy sheets have never been reported. To improve the productivity of the ISF process, a robust and efficient optimization framework is required to study the influence of input parameters on forming responses. Consequently, this research focuses on the formability study, the stress-based FFLD, and fracture behaviour of Mg alloys, as well as the optimization of process parameters during ISF.

In this study, four parameters, including spindle speed, tool diameter, vertical step depth, and feed rate, are considered based on preliminary experiments and CNC milling machine capabilities. This has prompted the authors to develop a combined experimental and optimization model to predict forming responses, such as formability and surface

roughness, which are dependent on spindle speed, tool diameter, vertical step depth, and feed rate. Finally, grey relational analysis (GRA) and fuzzy logic are combined to identify the important forming attributes influencing the ISF process for AZ31 material. Following this, strain-based forming fracture limit diagrams (FFLD) for Mg alloy were plotted, and fractographs were analysed to determine fracture behaviour.

## 2. Materials and Methods

This section discusses details of materials, preparation of blanks, experimental setup, DOE-based experimental procedure, and the optimization methods used.

### 2.1. Material

Sheets of the magnesium alloy AZ31 were used in the current work. When the sheet thickness is around 1 mm, the ISF process can be used efficiently [18]. Sheets of 1 mm thickness and 145 mm × 145 mm in size were used in this study. The material properties of AZ31 are 39.6 GPa Young's modulus, 1.77 g/cc density, and 246 MPa ultimate tensile strength. The chemical composition of AZ31 alloy is as shown in Table 1 below.

**Table 1.** Chemical compositions of magnesium alloy AZ31 sheets taken for this study.

| Component | Al | Mn | Si | Fe | Zn | Cu | Ni | Mg |
|---|---|---|---|---|---|---|---|---|
| Weight % | 3.1 | 0.31 | 0.035 | 0.0023 | 0.93 | 0.0015 | 0.00052 | Balance |

### 2.2. Experimental Setup

A conventional three-axis CNC milling machine capable of generating the required forming force (Model Maxmill Plus+, Sangli, Maharashtra, India) was used to perform the forming process. Using a clamping system, the raw material was held firmly in a machine fixture. In the study, hardened hemispherical-ended forming tools with diameters of 8 mm, 10 mm, and 12 mm are used and mounted on a rotating spindle along the *z*-axis.

Metal sheets, such as aluminium, and their alloys, are commonly formed using the ISF process because it is suitable for materials with good formability; however, forming magnesium and titanium alloys at room temperature is a complex task to achieve dimensional exactness and a superior surface finish. These materials are formed at high temperatures for these reasons. As a result, considering the previous literature [19], ISF for Mg alloys is performed at 250 degrees Celsius in this study.

Figure 1 illustrates the experimental setup of the ISF heating system. For the heating system and insulation design, great care was taken to avoid thermal gradients and achieve better temperature control around the sheet during the forming process. To heat the sheet, an induction coil system is designed and implemented. Throughout each experiment, the differences between the measured temperatures were never greater than 6 degrees Celsius. The heating system reaches the desired temperature more quickly.

### 2.3. Experimental Designs

In the experimental design, Taguchi L27 orthogonal arrays were used because Taguchi's experimental strategy provides robust design solutions, better quality, and an economical solution [20]. This method is capable of planning tests in an efficient manner, allowing for the collection of maximum data from fewer test runs. The following four process factors were considered for achieving higher formability and a good surface finish: (i) spindle speed (rpm), (ii) tool diameter (mm), (iii) tool feed rate (mm/min), and (iv) vertical step depth (mm), [21], with three levels for each factor, as shown in Table 2. Step depth gives us value by which next layer of forming will take place after one cycle of forming. In sheet forming, the forming strain is important, so measuring it is an important part of the ISF process.
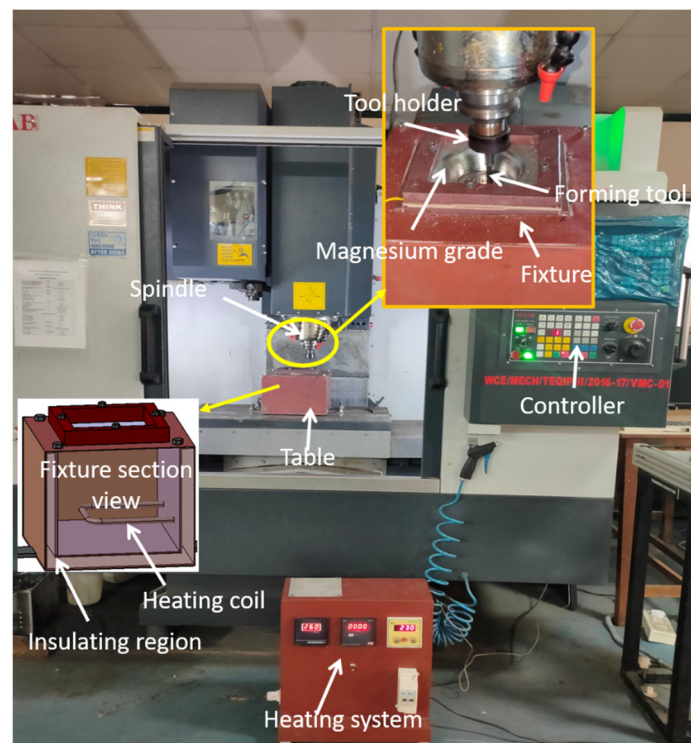
**Figure 1.** Experimental setup of ISF with the heating system.

**Table 2.** Parameters and their levels.

| Process Parameter | Units | Levels | | |
| --- | --- | --- | --- | --- |
| | | 1st | 2nd | 3rd |
| Tool diameter | mm | 8 | 10 | 12 |
| Feed rate | mm/min | 500 | 800 | 1000 |
| Spindle speed | rpm | 300 | 500 | 700 |
| Vertical step depth | mm | 0.3 | 0.5 | 0.7 |

To facilitate strain measurement, tiny circles with a diameter of 2 mm and a depth of 5 microns were engraved on one face of the sheet using a laser engraving machine in a rectangular array design. The engraved side of the sheet was fixed at the bottom, which was held by the fixture, during forming. As shown in Table 3, a total of 27 experiments with 4 factors and 3 levels were considered.

**Table 3.** Experimental plan.

| Sr. No. | Tool Diameter (mm) | Spindle Speed (rpm) | Step Depth (mm) | Feed Rate (mm/min) |
| --- | --- | --- | --- | --- |
| 1 | 8 | 300 | 0.3 | 500 |
| 2 | 8 | 300 | 0.5 | 800 |
| 3 | 8 | 300 | 0.7 | 1000 |
| 4 | 10 | 500 | 0.3 | 500 |
| 5 | 10 | 500 | 0.5 | 800 |
| 6 | 10 | 500 | 0.7 | 1000 |
| 7 | 12 | 700 | 0.3 | 500 |
| 8 | 12 | 700 | 0.5 | 800 |
| 9 | 12 | 700 | 0.7 | 1000 |
| 10 | 10 | 700 | 0.3 | 800 |
| 11 | 10 | 700 | 0.5 | 1000 |

**Table 3.** *Cont.*

| Sr. No. | Tool Diameter (mm) | Spindle Speed (rpm) | Step Depth (mm) | Feed Rate (mm/min) |
|---|---|---|---|---|
| 12 | 10 | 700 | 0.7 | 500 |
| 13 | 12 | 300 | 0.3 | 800 |
| 14 | 12 | 300 | 0.5 | 1000 |
| 15 | 12 | 300 | 0.7 | 500 |
| 16 | 8 | 500 | 0.3 | 800 |
| 17 | 8 | 500 | 0.5 | 1000 |
| 18 | 8 | 500 | 0.7 | 500 |
| 19 | 12 | 500 | 0.3 | 1000 |
| 20 | 12 | 500 | 0.5 | 500 |
| 21 | 12 | 500 | 0.7 | 800 |
| 22 | 8 | 700 | 0.3 | 1000 |
| 23 | 8 | 700 | 0.5 | 500 |
| 24 | 8 | 700 | 0.7 | 800 |
| 25 | 10 | 300 | 0.3 | 1000 |
| 26 | 10 | 300 | 0.5 | 500 |
| 27 | 10 | 300 | 0.7 | 800 |

Hussain [22] used the variable wall angle test model used in the SPIF process, which is the axis-symmetric part whose slope changes with depth, to check the maximum wall angle that could be reached by using ISF. Figure 2 shows variable angle tests sectional view.
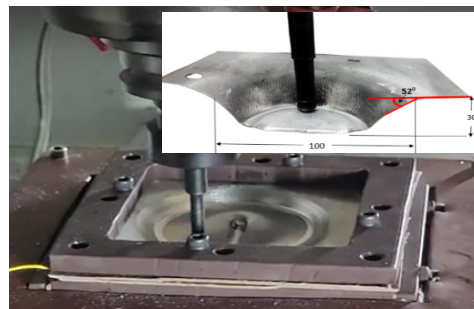


**Figure 2.** Sectional view of variable wall angle geometry.

The forming tool moves in horizontal and vertical planes according to the CNC program's predefined tool path and the variable wall angle cone-shaped part expected to be formed from the sheet blank. Similarly, one-by-one sheets were formed for 27 experiments.

*2.4. Measurement of Responses*

The output responses measured from these experiments are formability and surface roughness.

2.4.1. Surface Roughness Measurement

A Taylor Hobson Talysurf is used to measure surface roughness (Ra). For each experiment, the Ra value is measured at three distinct locations on the formed part, and the average of these measurements is considered the final value. Each experiment is replicated twice, and the mean of each response is recorded for the study.

2.4.2. Strain (Formability) Measurement

To measure the strain, a rectangular array of 2 mm diameter circles with a 5 micron depth was laser engraved. During incremental sheet forming, a single side of the sheet was engraved; this side was held in a fixture as the bottom side. After the formation process up to the fracture, these circles were elongated, and the major and minor diameters of nine circles surrounding the fracture were measured with a USB microscope for strain

calculation. Lastly, the forming fracture limit diagrams (FFLD) was plotted based on the strain values for each experiment. From these values, the major and minor true strains at the fracture zone were calculated, representing the strain-based forming limit. This method was repeated for each experiment. Using the calculated strain values, a strain-based FFLD was then plotted. Figure 3 shows a sheet deformed during the ISF process. Strain value and surface roughness were calculated using above mentioned procedure and shown in Table 4.
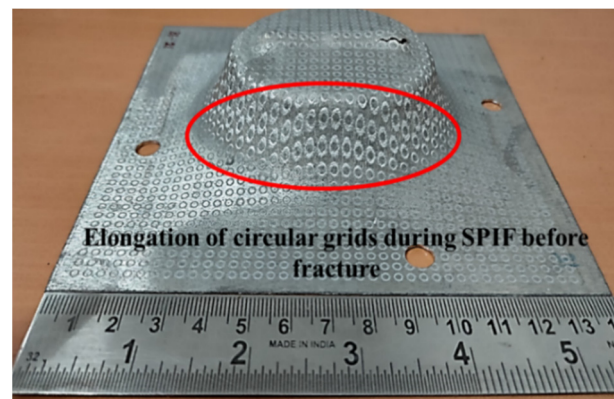


**Figure 3.** Deformed sheet during ISF process.

**Table 4.** Reponses measured from the experiments.

| Experiment Number | Strain | Surface Roughness (Micron) |
| --- | --- | --- |
| 1 | 1.740 | 2.415 |
| 2 | 1.613 | 2.557 |
| 3 | 1.315 | 3.157 |
| 4 | 1.905 | 2.468 |
| 5 | 1.675 | 2.640 |
| 6 | 1.435 | 3.125 |
| 7 | 1.955 | 2.500 |
| 8 | 1.855 | 2.756 |
| 9 | 1.495 | 3.256 |
| 10 | 1.970 | 2.524 |
| 11 | 1.585 | 2.604 |
| 12 | 1.859 | 3.122 |
| 13 | 1.825 | 2.465 |
| 14 | 1.376 | 2.506 |
| 15 | 1.525 | 2.957 |
| 16 | 1.735 | 2.623 |
| 17 | 1.424 | 2.635 |
| 18 | 1.575 | 3.125 |
| 19 | 1.695 | 2.454 |
| 20 | 1.680 | 2.356 |
| 21 | 1.710 | 2.965 |
| 22 | 1.800 | 2.744 |
| 23 | 1.856 | 2.722 |
| 24 | 1.775 | 3.305 |
| 25 | 1.694 | 2.435 |
| 26 | 1.726 | 2.400 |
| 27 | 1.646 | 3.018 |

## 2.5. Grey-Based Fuzzy Logic

This section describes, step-by-step, the grey-based fuzzy logic method for optimising the process. Figure 4 shows the procedure for the multi-response optimization used to determine the optimal combination of incremental sheet forming parameters for AZ31.
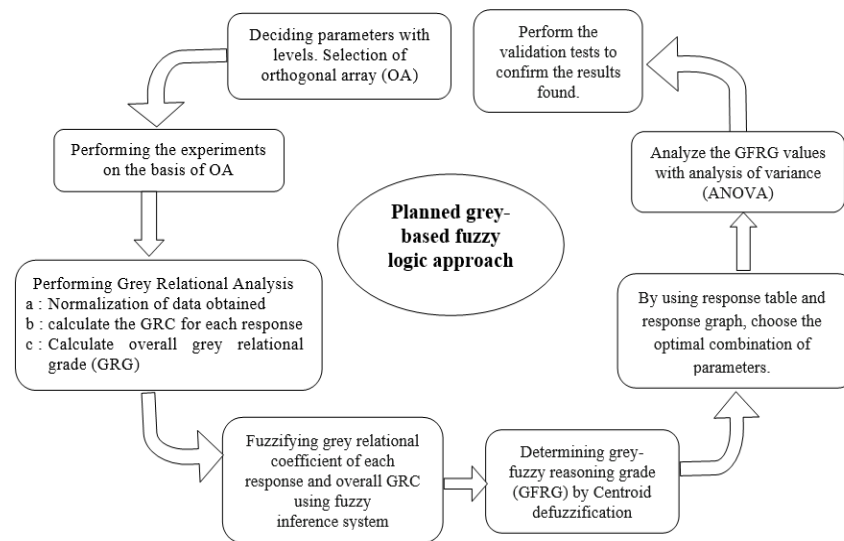
**Figure 4.** Steps used for the grey-fuzzy logic method.

### 2.5.1. Grey Relational Analysis (GRA)

In GRA, the various functions can be ignored if a value series for an output response variable is significant. As the response factors (formability and surface roughness) and units are not identical, it is necessary to pre-process the data to standardise the range, i.e., between 0 and 1. In the ISF process, the required formability must be high; therefore, the "larger the better" characteristic is preferred, whereas the surface roughness should be kept to a minimum by aiming for the "smaller the better" characteristic. The response variables were normalised using Equations (1) and (2), as follows:

$$x_i^*(n) = \frac{X_i(n) - \min X_i(n)}{\max X_i - \min X_i(n)} \tag{1}$$

$$x_i^*(n) = \frac{\max X_i(n) - X_i(n)}{\max X_i - \min X_i(n)} \tag{2}$$

where $X_i(n)$ is the normalised value, and $\min X_i(n)$ and $\max X_i(n)$ are the lowest and highest values of $X_i(n)$ for the nth response of it, respectively.

Equations (3) and (4) are used to figure out the grey relational coefficient (GRC) and grey relational grade (GRG) from the normalised value. Equation (3) is as follows:

$$GC_i(n) = \frac{\triangle_{\min} + \Phi_{\triangle_{\max}}}{\triangle_{0i}(n) + \Phi_{\triangle_{\max}}} \tag{3}$$

where $\Phi$ is the distinguishing coefficient 0.5 in this case, $GC_{ij}$ is the GRC value, and $\triangle_{0i}(n)$ is the mod difference between $X_i(n)$ to $X_j(n)$. Equation (4) is as follows:

$$G_i(n) = \frac{1}{n} \sum_{i=0}^{n} GC_i(n) \tag{4}$$

where 'n' is the number of process responses and $G_{ij}$ is grey relational grade. After calculating the grey relational grade (GRG), the maximum (GRG) value is considered optimal.

### 2.5.2. Fuzzy Grey Logic

The GRA categorises each response variable as lower-is-better, nominal-is-better, or higher-is-better. It analyses data and indicates a degree of uncertainty in the results. In this study, fuzzy logic will be used to estimate uncertainty [23].

For this study, a Mamdani fuzzy logic system is used. Its main components comprise the fuzzifier, its membership functions (MF), and rules based on a fuzzy inference engine

and fuzzified. Here, membership functions are used by the fuzzifier to fuzzify the GRC values (P1 = formability's grey relation coefficient, P2 = grey relation coefficient for roughness of surface), as it contains some grade of vagueness and ambiguity regarding performances characteristic. Then, input values (P1 and P2) and output (Q = GFRG) are mapped in the range of a 0 to 1 value with the help of the membership function. Afterwards, 27 fuzzy rules are defined by the following Equation (5) using GRC values of 2 inputs and 1 output:

$$\begin{aligned}
&\text{1st Rule: if P1 is Y1; and P2 is Z1, then Q is V1; else} \\
&\text{2nd Rule: if P1 is Y2; and P2 is Z2, then Q is V2; else} \\
&\text{nth Rule: if P1 is Yn, and P2 is Zn, Q is Vn.}
\end{aligned} \tag{5}$$

where Yi, Zi, and Vi are subsets of fuzzy value stated through a respective membership function.

An inference engine calculates the fuzzy value based on fuzzy rules upon which fuzzy reasoning is performed. In the final step, the grey-fuzzy reasoning grade (GFRG) is predicted, which is a single value that describes equivalent multi-performance characteristics using fuzzy defuzzification with the following Equation (6):

$$\mu_{(C_0)} = ((\mu_{(Y_1)}(P1) \wedge (\mu_{(Z_1)}(P2) \wedge (\mu_{(V_1)}(Y)) \vee \ldots ((\mu_{(Y_n)}(Pn) \wedge (\mu_{(Z_n)}(Pn)) \wedge (\mu_{(V_1)}(Y)) \tag{6}$$

Finally, the fuzzy values are converted into crisp output using a defuzzifier, as in the following Equation (7):

$$Y_0 = \frac{\sum Y \, \mu_{C_0}(Y)}{\sum \mu_{C_0}(Y)} \tag{7}$$

### 2.6. ANOVA for GFRG

Here, ANOVA is useful for identifying input variables that significantly influence the response variable. The ANOVA is a mathematical method for attributing output variability to distinct types of inputs. The complete disparity between GFRG is computed using the deviations in the sum of the squares from the total mean of GFRG. Then, these values are de-integrated into the following two bases: the sum of square deviations caused by each forming factor and the sum of squared errors. Finally, significant forming parameters that have a major impact on the GFRG were identified.

### 3. Results and Discussion

### 3.1. Strain Based FFLD

Sheet metal is subjected to plane strain and biaxial tension strain conditions during incremental forming. The surface roughness and formability of the sheets vary under these conditions. When the sum of the major and minor strains in plane strain is compared to the sum of the strains in biaxial tension, the sum of the strains in plane strain is greater. This is due to the rapid rate of thinning caused by stretching in both axes. Figure 5 depicts the strain-based FFLD for all the experiments. It varies significantly from the curve used in conventional forming. In the biaxial strain region, it appears as a straight line with a negative slope.

There is no negative strain (compressive strain) at any location on the formed part. The reason for this is that the ball-ended tool presses the sheet metal locally under its surface, causing a very small deformation. Because of the nature of the ball-ended tool's movement, in which the tool first penetrates the sheet metal and moves in one direction, the metal always flows away from the tool, which is also in the direction of the tool movement. As a result, the negative strain is not present at any stage.
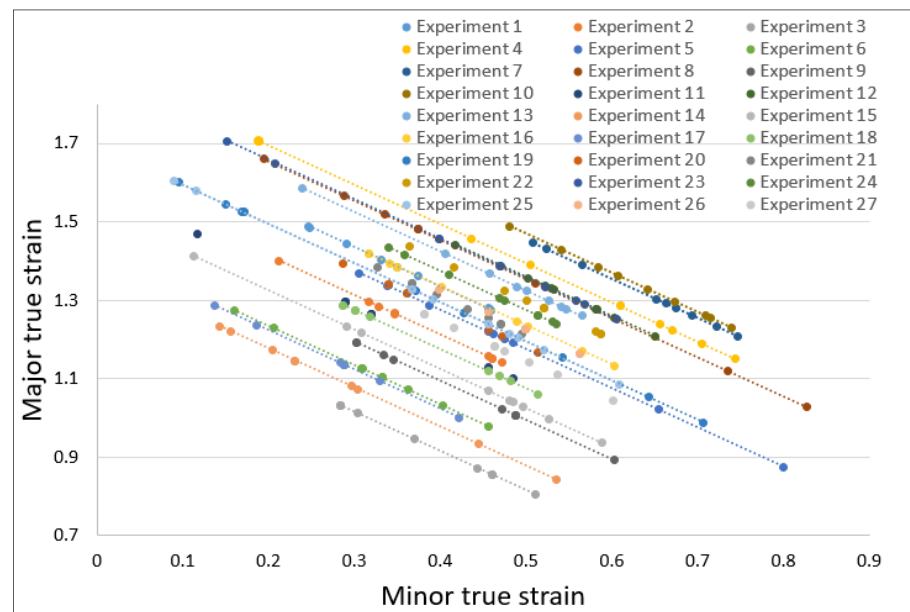
**Figure 5.** Strain-based FFLD for AZ31 Mg alloy.

The FFLD for the Mg AZ31 alloy sheet was plotted with major and minor strain values for each experiment and presented in Figure 6. Experiment number 10 had the highest formability; experiment number 27 had a medium formability; experiment number 3 had the least formability, as shown in Figure 5. Combining parameters, such as medium tool diameter, low vertical step depth, medium feed rate, and high spindle speed increases the sample's formability. The medium formability blank was machined with the following parameters: a medium tool diameter, a high vertical step depth, a medium feed rate, and a low spindle speed. The experiment sample with the lowest formability was machined using the parameters with the smallest tool diameter, the highest vertical step depth, the highest feed rate, and the lowest spindle speed.
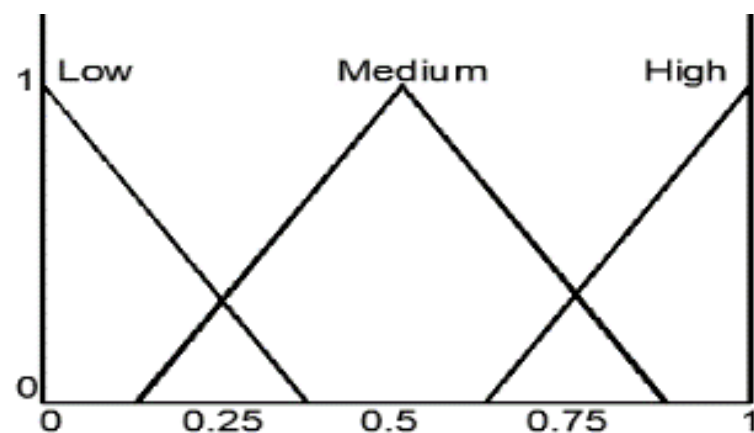


**Figure 6.** Membership functions of input.

The average strain sums for high, medium, and low formability samples are 1.431, 1.266, and 0.972, respectively. The sample with the highest formability has a forming limit that is 13.03% greater than the sample with moderate formability and 30.24 % greater than the sample with the lowest formability.

*3.2. Optimization*

The normalised experimental data, grey relational coefficients for both responses, and GR grade for each experiment are displayed in Table 5. A MATLAB (R2019b) fuzzy logic

tool is used to calculate the grey-fuzzy reasoning grade (GFRG). As input, the fuzzy logic system received the GR coefficients of formability and surface roughness. The membership function of the triangular shape was used for fuzzy modelling. Three linguistic membership functions, namely HIGH, MEDIUM, and LOW, were used to represent the grey relational coefficients (GRC) of the input variable. As shown in Figures 6 and 7, the membership functions LOWEST, VERY LOW, LOW, MEDIUM, HIGHER, VERY HIGHER, and HIGHEST are used to represent the output, i.e., the overall grey relational grade.

**Table 5.** Pre-processed data, grey relational coefficients, and grey relational grade AZ31.

| Experiment No | Normalised Experimental Data (Data Pre-Processing) | | Grey Relational Coefficient | | Grey Relational Grade |
|---|---|---|---|---|---|
| | Formability | Surface Roughness | Formability | Surface Roughness | |
| 1. | 0.6929 | 0.9272 | 0.6195 | 0.8728 | 0.7462 |
| 2. | 0.5053 | 0.7589 | 0.5027 | 0.6747 | 0.5887 |
| 3. | 0.0000 | 0.1359 | 0.3333 | 0.3665 | 0.3499 |
| 4. | 0.9170 | 0.8628 | 0.8576 | 0.7846 | 0.8211 |
| 5. | 0.5987 | 0.6645 | 0.5547 | 0.5984 | 0.5766 |
| 6. | 0.2161 | 0.1655 | 0.3894 | 0.3747 | 0.3820 |
| 7. | 0.9874 | 0.8249 | 0.9754 | 0.7407 | 0.8581 |
| 8. | 0.8512 | 0.5368 | 0.7706 | 0.5191 | 0.6449 |
| 9. | 0.3174 | 0.0441 | 0.4228 | 0.3434 | 0.3831 |
| 10. | 1.0000 | 0.7973 | 1.0000 | 0.7115 | 0.8558 |
| 11. | 0.4620 | 0.7044 | 0.4817 | 0.6284 | 0.5551 |
| 12. | 0.8569 | 0.1683 | 0.7775 | 0.3755 | 0.5765 |
| 13. | 0.8109 | 0.8666 | 0.7255 | 0.7894 | 0.7575 |
| 14. | 0.1138 | 0.8180 | 0.3607 | 0.7331 | 0.5469 |
| 15. | 0.3665 | 0.3292 | 0.4411 | 0.4271 | 0.4341 |
| 16. | 0.6857 | 0.6827 | 0.6140 | 0.6117 | 0.6129 |
| 17. | 0.1970 | 0.6695 | 0.3837 | 0.6021 | 0.4929 |
| 18. | 0.4464 | 0.1655 | 0.4745 | 0.3747 | 0.4246 |
| 19. | 0.6280 | 0.8803 | 0.5734 | 0.8068 | 0.6901 |
| 20. | 0.6060 | 1.0000 | 0.5593 | 1.0000 | 0.7797 |
| 21. | 0.6498 | 0.3208 | 0.5881 | 0.4240 | 0.5061 |
| 22. | 0.7771 | 0.5497 | 0.6917 | 0.5262 | 0.6089 |
| 23. | 0.8536 | 0.5738 | 0.7735 | 0.5399 | 0.6567 |
| 24. | 0.7421 | 0.0000 | 0.6597 | 0.3333 | 0.4965 |
| 25. | 0.6267 | 0.9028 | 0.5725 | 0.8372 | 0.7049 |
| 26. | 0.6733 | 0.9462 | 0.6048 | 0.9028 | 0.7538 |
| 27. | 0.5561 | 0.2689 | 0.5297 | 0.4062 | 0.4679 |
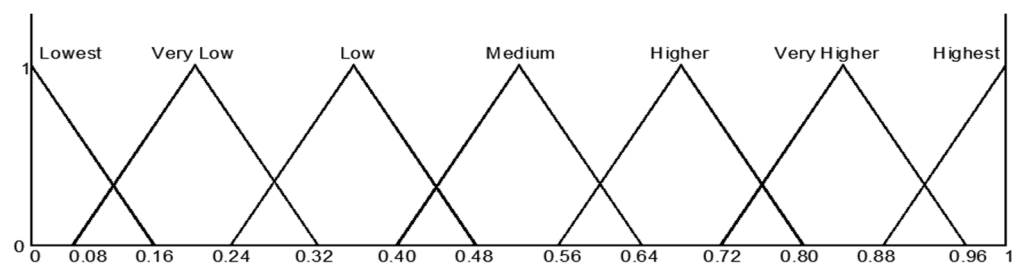


**Figure 7.** Membership functions for multi-response output.

Table 5 presents the normalised S/N ratios for surface roughness and formability. Normalization has been performed because the S/N range has a dissimilar range and trend; therefore, pre-processing of data is necessary. In Table 5, the GRC for AZ31 was calculated for both responses. The GRG and GRFC values are used for a comprehensive

analysis of multi-objective characteristics. The greater the GRFG value, the more significant the influence.

Figure 8 shows the fuzzy logic reasoning graphically; first, two columns represent input parameters, i.e., GRC values of formability and surface roughness, respectively, and finally, defuzzied GFRG is represented in the last column. Twenty-seven rows represent the twenty-seven fuzzy rules. The input values given to get GFRG are GRC for formability and surface roughness. In the first experiment, the GRC values for formability and surface roughness are 0.62 and 0.873, respectively. For the first experiment, the defuzzified output of the GFRG value is 0.745 (Figure 8).
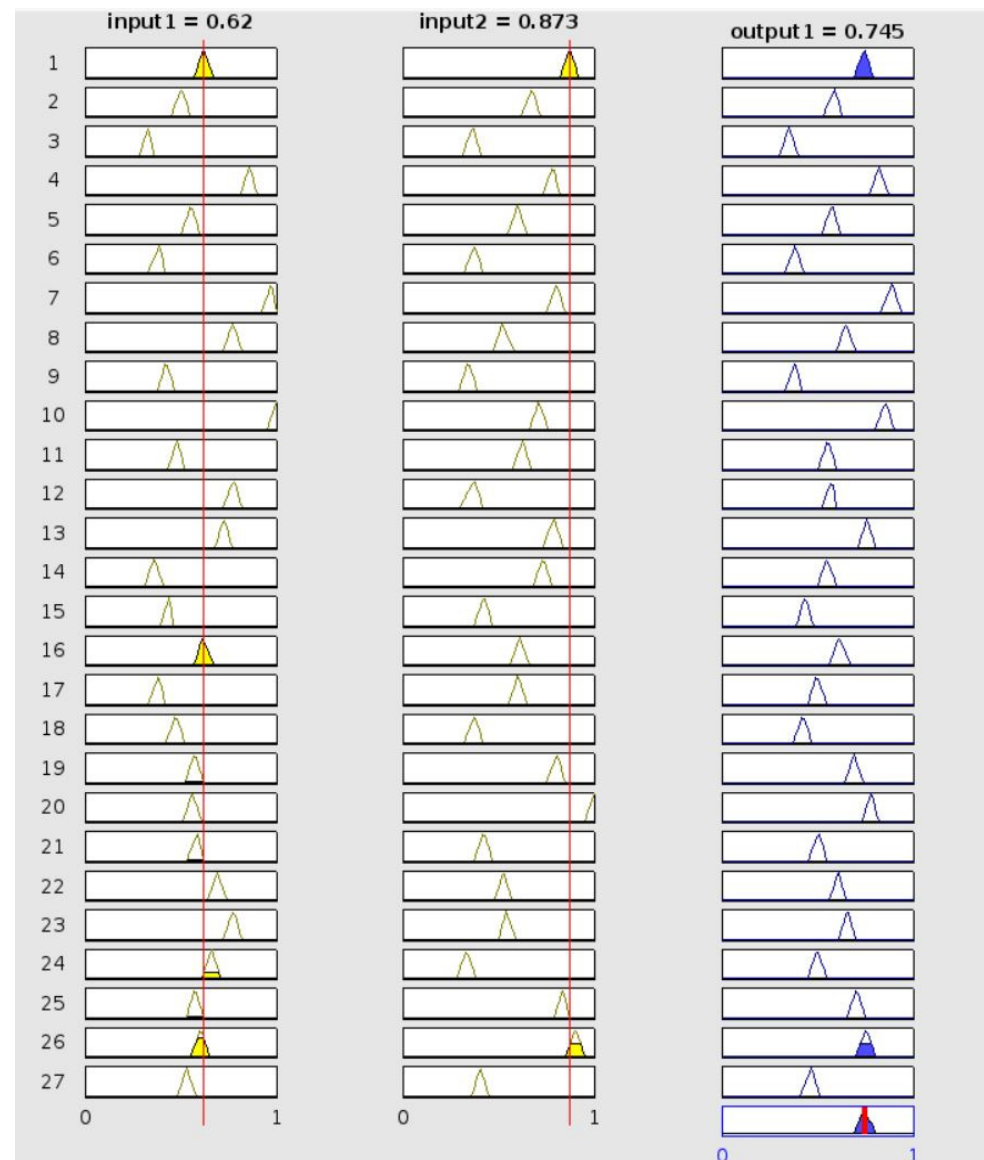


**Figure 8.** Fuzzy logic rules viewer for Experiment No. 1.

According to Table 6, among the 27 experiments, Experiment No. 7 has the highest multiple performance characteristics, as measured by the highest GFR grade (highlighted). As previously stated, the higher the value of GFRG, the closer the optimal parameter combination is; thus, it is the optimal combination.

**Table 6.** Grey-fuzzy reasoning grades (GRFC) and rank.

| Experiment Number | Grey-Fuzzy Reasoning Grade (GFRG) | GFRG Based Rank |
|---|---|---|
| 1. | 0.745 | 7 |
| 2. | 0.583 | 14 |
| 3. | 0.352 | 27 |
| 4. | 0.82 | 3 |
| 5. | 0.572 | 15 |
| 6. | 0.381 | 25 |
| 7. | 0.853 | 1 |
| 8. | 0.649 | 11 |
| 9. | 0.381 | 25 |
| 10. | 0.852 | 2 |
| 11. | 0.557 | 17 |
| 12. | 0.565 | 16 |
| 13. | 0.757 | 5 |
| 14. | 0.549 | 18 |
| 15. | 0.435 | 23 |
| 16. | 0.614 | 12 |
| 17. | 0.498 | 21 |
| 18. | 0.422 | 24 |
| 19. | 0.693 | 9 |
| 20. | 0.777 | 4 |
| 21. | 0.502 | 19 |
| 22. | 0.606 | 13 |
| 23. | 0.651 | 10 |
| 24. | 0.499 | 20 |
| 25. | 0.702 | 8 |
| 26. | 0.748 | 6 |
| 27. | 0.463 | 22 |

Using the delta statistic, which is based on the difference between the lowest and highest average GFRG value for individual factors, Table 7 ranks the input factors that influence the output response. The step depth has the greatest impact on the output response characteristics, followed by the feed rate, tool diameter, and spindle speed (Table 7).

**Table 7.** Response of GFRG.

| Process Parameters | Levels | | | Maximum Value-Minimum Value | Rank |
|---|---|---|---|---|---|
| | 1 | 2 | 3 | | |
| Tool diameter (mm) | 0.5522 | 0.6289 | 0.6218 | 0.0767 | 3 |
| Spindle speed (rpm) | 0.5927 | 0.5866 | 0.6237 | 0.0371 | 4 |
| Step depth (mm) | 0.7380 | 0.6204 | 0.4444 | 0.2936 | 1 |
| Feed rate (mm/min) | 0.6684 | 0.6101 | 0.5243 | 0.1441 | 2 |

Average value GFRG for optimal parameter levels =0.665.

Here, ANOVA is used to examine the influence of all four following input parameters on the experimental outcomes: spindle speed, tool diameter, vertical step depth, and feed. Step depth is the most influential parameter (contributing 68.78%), and feed rate is the second most influential parameter (contributing 16.56%), as shown in Table 8 of the ANOVA results, echoing the findings of the current literature [24].

For the confirmation experiment, the highest GRFC values are regarded as the best parameters. For AZ31, the optimal process levels are tool diameter level 2, spindle speed level 3, step depth level 1, and feed rate level 1 (i.e., TD2SS3SD1FR1). Figure 9 depicts the average effect plot for roughness and strain.

**Table 8.** ANOVA of GFRG.

| Parameters | DOF | Adj SS | Adj MS | F-Value | *p*-Value | Significant |
|---|---|---|---|---|---|---|
| Tool diameter | 2 | 0.032299 | 0.016149 | 6.57 | 0.007 | Significant |
| Spindle speed | 2 | 0.007127 | 0.003563 | 1.45 | 0.261 | Non-significant |
| Feed rate | 2 | 0.094586 | 0.047293 | 19.25 | 0.000 | Significant |
| Step depth | 2 | 0.392911 | 0.196455 | 79.97 | 0.000 | Significant |
| Error | 18 | 0.044221 | 0.002457 | - | - | - |
| Total | 26 | 0.571143 | - | - | - | - |
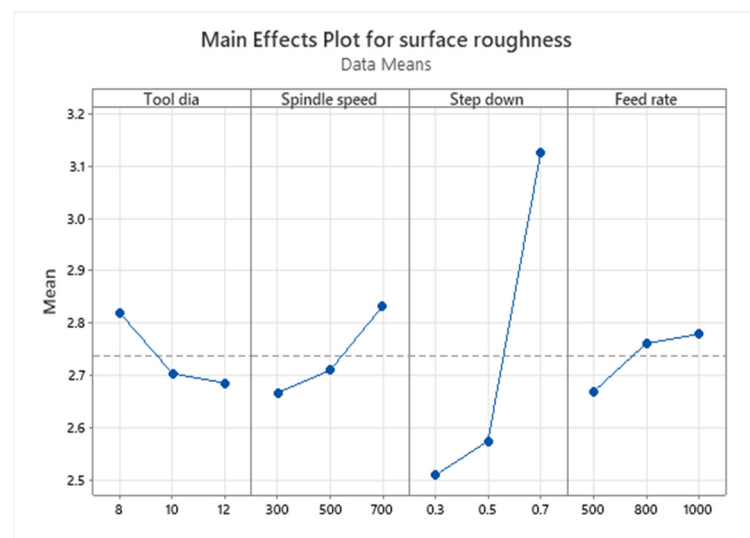


(**a**)
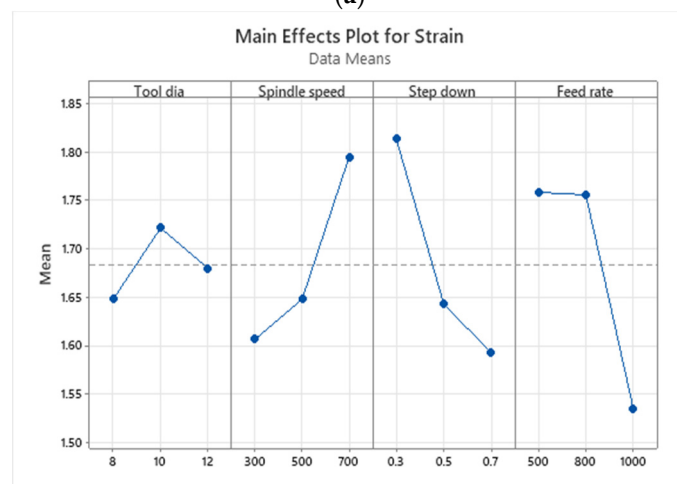


(**b**)

**Figure 9.** Mean effect plot for (**a**) surface roughness and (**b**) strain.

### 3.3. Effect of Input Parameter

Figure 9a shows that as the tool diameter increases, the surface roughness value decreases. A larger tool diameter allows for more surface contact between the tool and the sheet, resulting in a smoother surface finish. As shown in Figure 9b, as the tool's diameter increases, strain increases to a certain limit before decreasing. This is due to the fact that the area of contact when using an 8 mm tool is very small, making it more likely to cause a crack along the forming direction. When the diameter of the tool increases, so does the area of contact, which reduces the material's formability.

As Figure 9a shows, the surface finish appears to deteriorate as spindle speed, and this could be because the momentary sticking increases with speed. Figure 9b shows that the strain value increases as spindle speed increases. A higher spindle speed causes more localised heating of the interface between the tool and the sheet, which in turn increases ductility in that specific area. The sheet was easily shaped when the swivelling motion was induced by spindle rotation. Consequently, forming with a greater swivelling action enhanced formability compared to forming with a straight motion.

In addition, the surface finish appears to deteriorate as the step depth increase, because of the high strength and strain hardening index of this material. The effect of the spring back effect and strain hardening is increased when the vertical step depth is increased in magnitude. This effect of strain hardening and spring back increases the severity of the formation. Consequently, the total strain value decreases.

Owing to the high strength and high strain hardening index value of Mg alloy, strain value increases as feed rate increases. In general, lowering the vertical step depth and feed rate reduces forming severity and strain hardening. Consequently, reducing the vertical step depth and feed rate increases formability.

The optimal strain is achieved with a medium tool diameter, the lowest step depth, the highest spindle speed, and the lowest feed rate. The highest tool diameter, lowest step depth, lowest spindle speed, and lowest feed rate produce the best surface finish. The findings indicate that formability increases when spindle speed, vertical step depth, and feed rate are increased. Vignesh et al. [25] discovered a similar trend in their study.

### 3.4. Confirmation Experiment

In order to validate it, the experiment was conducted with optimal parameter levels. This experiment yields the highest GRFG, confirming that the process parameters of TD2SS3SD1FR1 are optimal. Table 9 contains the results of confirmatory tests, the optimal level of process parameters, and the improvement percentage. The GRFG values increased from 0.853 to 0.882, a 3.4% increase. Figure 10 demonstrates that the forming limit area for optimised parameters is greater than the forming limit area for the first rank experiment.

**Table 9.** Results of ISF in confirmation test.

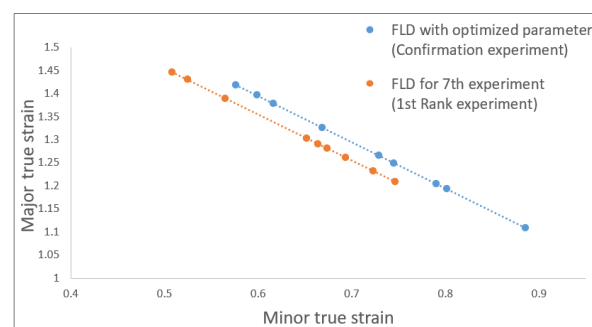| Response | Orthogonal Trial No. 7 | Optimal Machining Parameters Using TGRA | |
| --- | --- | --- | --- |
| | | **Predicted** | **Experiment** |
| Level | TD3 SS3 SD1 FR1 | TD2 SS3 SD1 FR1 | TD2 SS3 SD1 FR1 |
| Strain | 1.955 | - | 1.995 |
| Surface roughness (micron) | 2.5 | - | 2.235 |
| Grey relational fuzzy grade (GRFG) | 0.853 | 0.856 | 0.882 |



**Figure 10.** FFLD for first rank and confirmation experiment.

### 3.5. SEM Analysis

The fractured surfaces of the chosen samples were examined using SEM (higher, moderate, and least formability). Figure 11 illustrates the fractographs of three representative

samples with different magnifications. In general, there are three types of voids, namely spherical, prolate (when the void grows in the thickness direction), and oblate (when the void grows in the length or width direction) [26]. Figure 11a depicts the dimple fracture identified as the mode of fracture for the sample with greater formability. The majority of voids on this fractured surface are prolate. Due to the dimple fracture, a greater number of voids are created, which aggregate to demonstrate that the fracture is ductile. Due to more voids forming, the sheet's forming limit has increased significantly.
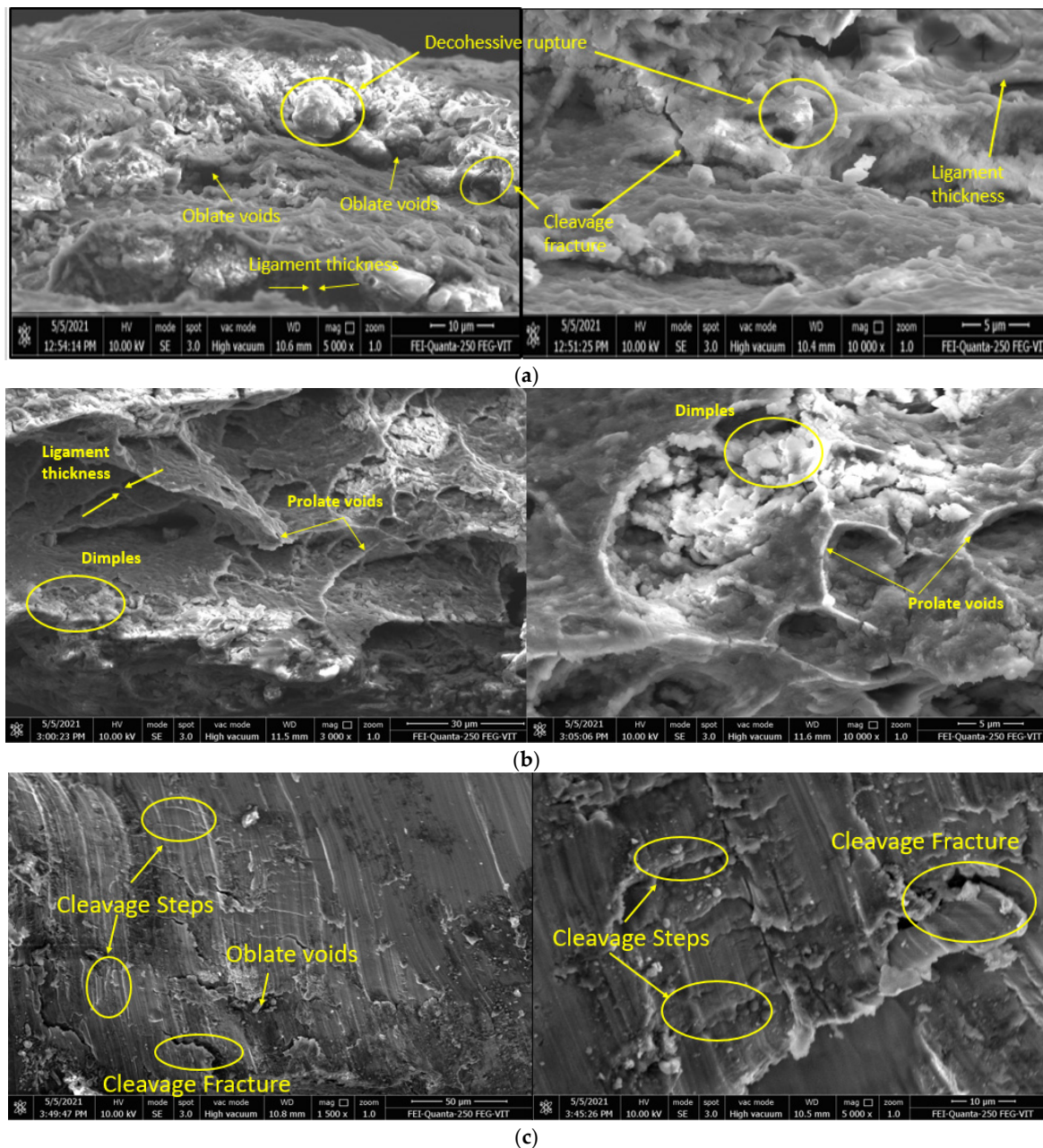


**Figure 11.** SEM images of a fractured surface of a sample at different magnifications, with (**a**) highest formability, (**b**) medium formability, and (**c**) least formability.

The fracture mode for the sample with moderate formability was observed as a cleavage fracture, as shown in Figure 11b. Both oblate and prolate void types can be found in this cracked surface. Figure 11 depicts the specific number of voids that become nucleated and consolidate with one another (b). Due to an average number of void formations, the sheet's forming limit has only been slightly increased. As shown in Figure 11c, the fracture

mode for the sample with the lowest formability was a cleavage fracture and decohesive rupture. On this fractured surface, the majority of the voids are oblate. Because of the decohesive rupture, fewer voids nucleate and coalesce. Because there are fewer void formations, the sheet's forming limit is simply constrained.

*3.6. Finite Element Simulation*

The FE simulation of ISF process has been carried out to check whether or not the ISF process is feasible to model with the FE package. For this, FE simulation of the ISF process for magnesium AZ31 alloy was carried out with optimised parameters and levels to compare the strain value obtained from experimentation (confirmation experiment) and from FE simulation. In this work, a full three-dimensional (3D) FE model of the SPIF process is created. For this work, the LS Dyna 7.0 software package was used, and a thorough analysis was carried out. Because of the formation of large strain plasticity, the requirement for complex tool paths, and the difficulty in developing contacts, FE simulation of the ISF process is complex.

Here, FE modeling has been carried out using the following steps: (1) Create parts with mesh i.e., a plate is created for the sheet blank and a sphere is created for the tool. Shell elements of 1 mm size are used to mesh the sheet as well as tool in this study. (2) Define the material models and assign the material to the section; two materials are created, one of which is for the sheet which consists of density($\rho$) 1.77 g/cc, Young's modulus (E) 39.6 GPa, Poisson's ratio 0.35, strength coefficient (k) 292MPa, and strain hardening index (n) 0.184 [27], and the second one is for the tool. (3) The tool position is set using the translate option, and the tool is considered a rigid body in this case because it is the only sheet that will be deformed into a permanent shape; its behaviour is referred to as "power law plasticity" in the ISF process. (4) Define the interaction behaviour between the tool and blank; as the tool and sheet are in constant contact, the contact condition "FORMING ONE WAY SURFACE TO SURFACE" was chosen. (5) Define the tool movement path and boundary conditions; this FE model provides motion to the tool as a spiral curve with decreasing diameter that moves as a rigid body with all ends of the sheets fixed; the model imposes these boundary conditions. For FE simulation, a variable wall angle cone shape was used; here, as depth increases, the diameter of the cup decreases. (6) Submit model to run and analyze the results using a post-processor. Figure 12 shows the simulated FE model.

Sheets can be formed in less time during ISF by increasing the stepdown or step depth. Because of the material behaviours, such as the high strain hardening index and high strength, step depth is the most influential parameter. However, if the step depth is increased too much, the sheet will easily fracture. The third most influential parameter is tool diameter; as tool diameter increases, the surface contact between tool and sheet increases, which increases friction, as shown in Figure 13.

Furthermore, as friction between the tool and the sheet increases, tool pressure increases, reducing sheet stress. As the formation of the crack is delayed, its formability improves. The mean effect plot shows that if the friction between the tool and the sheet increases excessively, the sheet will fracture [28].

Figure 14 depicts the ISF process simulation's plastic strain plot. The FE simulation yielded a strain value of 1.958, which is very close to the strain value obtained from the confirmation experiment (1.995).
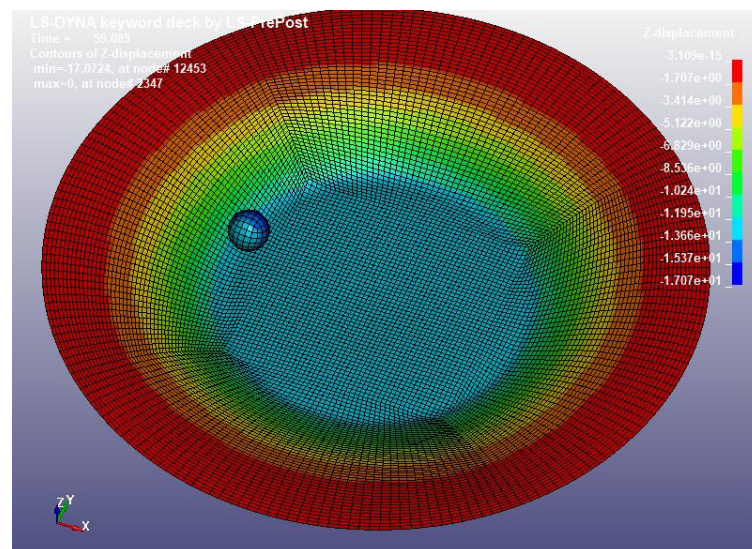
**Figure 12.** Simulated FE model with Z-direction displacement contour plot.
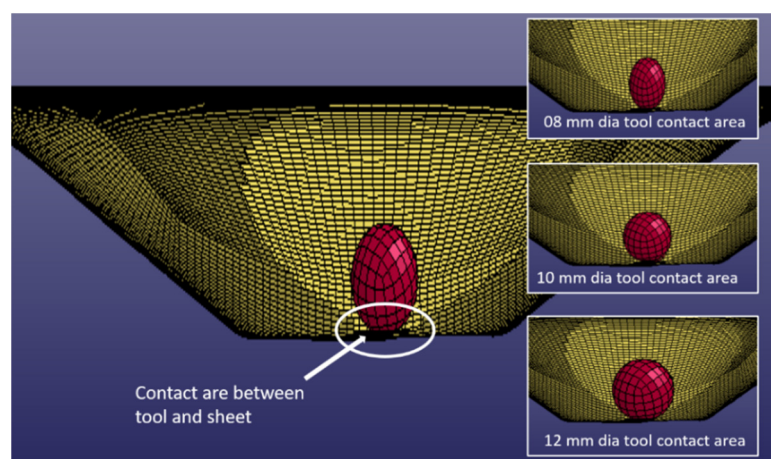


**Figure 13.** A contact area between tool and sheet for different tool diameters.
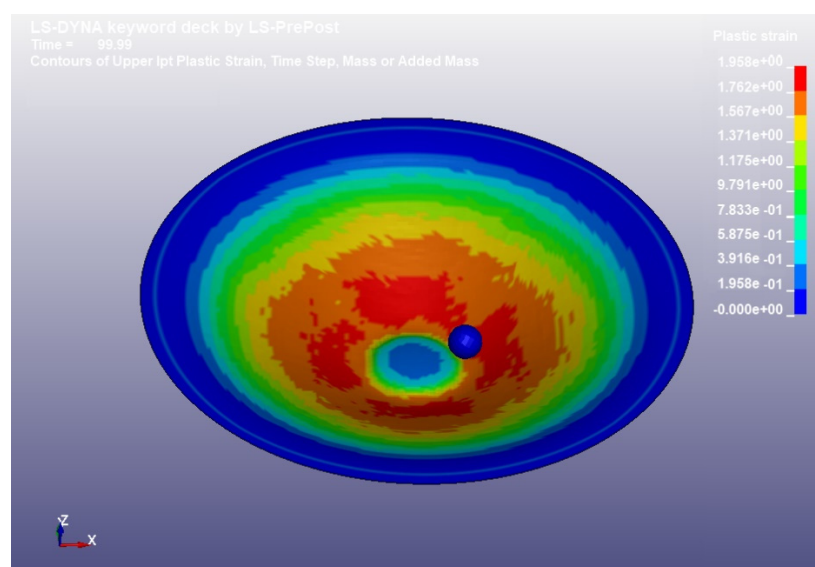


**Figure 14.** Plastic strain plot of ISF process simulation.

## 4. Conclusions

This study was conducted to better understand the critical forming factors for Mg alloy, specifically formability and roughness during the warm ISF process. The optimum process parameters for AZ31 Mg alloy are a feed rate of 500 mm/min, tool diameter of 10 mm, vertical step depth of 0.3 mm, and spindle speed of 700 rpm. Furthermore, step depth was discovered to be the primary contributing parameter, accounting for 68.78% of the total. Feed rate and tool diameter were identified as the second and third contributing factors, respectively, with spindle speed being the least important.

The confirmatory experiment results revealed that the grey-fuzzy optimised forming factor values yielded the best results for AZ31 during the ISF process. The confirmation experiment and FE simulation strain values are very close, with less than a 2% error margin.

The formability of the AZ31 sheet was positively influenced by spindle speed and negatively influenced by feed rate and vertical step depth in the SPIF process, according to strain-based FFLD. The swivelling action was responsible for the spindle speed benefit. Because of forming and strain hardening, feed rate and vertical step depth had unfavourable effects.

The fractured surface of the sample with the highest formability has prolate voids and a dimple fracture mode. The fractographs revealed that the samples with moderate and low formability have oblate voids and, on the fractured surface, decohesive and cleavage fracture rupture modes.

**Author Contributions:** R.M. designed and performed the experiment and collected data. P.C. was responsible for the optimization and fracture behaviour study. All authors have read and agreed to the published version of the manuscript.

**Institutional Review Board Statement:** Not applicable.

**Informed Consent Statement:** Not applicable.

**Data Availability Statement:** The data presented in this study are available on request from the corresponding author.

**Conflicts of Interest:** The authors declare no conflict of interest.

## References

1. Raju, C.; Sathiya Narayanan, C. Application of a Hybrid Optimization Technique in a Multiple Sheet Single Point Incremental Forming Process. *Meas. J. Int. Meas. Confed.* **2016**, *78*, 296–308. [CrossRef]
2. Pandivelan, C.; Jeevanantham, A.K. Formability Analysis of Al 5052 in Single Point Incremental Forming. *Int. J. Appl. Eng. Res.* **2014**, *9*, 337–386.
3. Yoganjaneyulu, G.; Sathiya Narayanan, C.; Narayanasamy, R. Investigation on the Fracture Behavior of Titanium Grade 2 Sheets by Using the Single Point Incremental Forming Process. *J. Manuf. Process.* **2018**, *35*, 197–204. [CrossRef]
4. Zhang, Q.; Guo, H.; Xiao, F.; Gao, L.; Bondarev, A.B.; Han, W. Influence of Anisotropy of the Magnesium Alloy AZ31 Sheets on Warm Negative Incremental Forming. *J. Mater. Process. Technol.* **2009**, *209*, 5514–5520. [CrossRef]
5. Park, J.; Kim, J.; Park, N.; Kim, Y. Study of Forming Limit for Rotational Incremental Sheet Forming of Magnesium Alloy Sheet. *Metall. Mater. Trans. A Phys. Metall. Mater. Sci.* **2010**, *41*, 97–105. [CrossRef]
6. Ji, Y.H.; Park, J.J. Incremental Forming of Free Surface with Magnesium Alloy AZ31 Sheet at Warm Temperatures. *Trans. Nonferrous Met. Soc. China* **2008**, *18*, 165–169. [CrossRef]
7. Van Sy, L.; Nam, N. Effect of Strain Rate and Temperature on Formability of Warm Incremental Forming Process with Magnesium Alloy Sheet AZ31. *J. Manuf. Technol. Res.* **2015**, *6*, 17–31.
8. Duflou, J.R.; Callebaut, B.; Verbert, J.; De Baerdemaeker, H. Laser Assisted Incremental Forming: Formability and Accuracy Improvement. *CIRP Ann.—Manuf. Technol.* **2007**, *56*, 273–276. [CrossRef]
9. Attanasio, A.; Ceretti, E.; Giardini, C.; Mazzoni, L. Asymmetric Two Points Incremental Forming—Improving Surface Quality and Geometric Accuracy by Tool Path Optimization. *J. Mater. Process. Technol.* **2008**, *197*, 59–67. [CrossRef]
10. Ambrogio, G.; De Napoli, L.; Filice, L.; Gagliardi, F.; Muzzupappa, M. Application of Incremental Forming Process for High Customised Medical Product Manufacturing. *J. Mater. Process. Technol.* **2005**, *162–163*, 156–162. [CrossRef]
11. Zhang, K.F.; Yin, D.L.; Wu, D.Z. Formability of AZ31 Magnesium Alloy Sheets at Warm Working Conditions. *Int. J. Mach. Tools Manuf.* **2006**, *46*, 1276–1280. [CrossRef]

12. Ambrogio, G.; Filice, L.; Manco, G.L. Warm Incremental Forming of Magnesium Alloy AZ31. *CIRP Ann.—Manuf. Technol.* **2008**, *57*, 257–260. [CrossRef]

13. Chino, Y.; Kimura, K.; Hakamada, M.; Mabuchi, M. Mechanical Anisotropy Due to Twinning in an Extruded AZ31 Mg Alloy. *Mater. Sci. Eng. A* **2008**, *485*, 311–317. [CrossRef]

14. Kleiner, S.; Uggowitzer, P.J. Mechanical Anisotropy of Extruded Mg-6% Al-1% Zn Alloy. *Mater. Sci. Eng. A* **2004**, *379*, 258–263. [CrossRef]

15. Wu, H.Y.; Zhou, G.Z.; Gao, Z.W.; Chiu, C.H. Mechanical Properties and Formability of an Mg-6%Li-1%Zn Alloy Thin Sheet at Elevated Temperatures. *J. Mater. Process. Technol.* **2008**, *206*, 419–424. [CrossRef]

16. Pandey, R.K.; Panda, S.S. Optimization of Bone Drilling Parameters Using Grey-Based Fuzzy Algorithm. *Meas. J. Int. Meas. Confed.* **2014**, *47*, 386–392. [CrossRef]

17. Das, B.; Roy, S.; Rai, R.N.; Saha, S.C. Application of Grey Fuzzy Logic for the Optimization of CNC Milling Parameters for Al–4.5%Cu–TiC MMCs with Multi-Performance Characteristics. *Eng. Sci. Technol. Int. J.* **2016**, *19*, 857–865. [CrossRef]

18. Baruah, A.; Pandivelan, C.; Jeevanantham, A.K. Optimization of AA5052 in Incremental Sheet Forming Using Grey Relational Analysis. *Measurement* **2017**, *106*, 95–100. [CrossRef]

19. Kim, S.W.; Lee, Y.S.; Kang, S.H.; Lee, J.H. Incremental Forming of Mg Alloy Sheet at Elevated Temperatures. *J. Mech. Sci. Technol.* **2007**, *21*, 1518–1522. [CrossRef]

20. Mia, M.; Dey, P.R.; Hossain, M.S.; Arafat, M.T.; Asaduzzaman, M.; Shoriat Ullah, M.; Tareq Zobaer, S.M. Taguchi S/N Based Optimization of Machining Parameters for Surface Roughness, Tool Wear and Material Removal Rate in Hard Turning under MQL Cutting Condition. *Meas. J. Int. Meas. Confed.* **2018**, *122*, 380–391. [CrossRef]

21. Leonhardt, A.; Kurz, G.; Victoria-Hernández, J.; Kräusel, V.; Landgrebe, D.; Letzig, D. Experimental Study on Incremental Sheet Forming of Magnesium Alloy AZ31 with Hot Air Heating. *Procedia Manuf.* **2018**, *15*, 1192–1199. [CrossRef]

22. Hussain, G.; Gao, L. A Novel Method to Test the Thinning Limits of Sheet Metals in Negative Incremental Forming. *Int. J. Mach. Tools Manuf.* **2007**, *47*, 419–435. [CrossRef]

23. Pattnaik, S.; Karunakar, D.B.; Jha, P.K. Multi-Characteristic Optimization of Wax Patterns in the Investment Casting Process Using Grey-Fuzzy Logic. *Int. J. Adv. Manuf. Technol.* **2013**, *67*, 1577–1587. [CrossRef]

24. Ambrogio, G.; Filice, L.; Gagliardi, F. Improving Industrial Suitability of Incremental Sheet Forming Process. *Int. J. Adv. Manuf. Technol.* **2012**, *58*, 941–947. [CrossRef]

25. Vignesh, G.; Narayanan, C.S.; Pandivelan, C.; Shanmugapriya, K.; Tejavath, B.N.; Tirupathi, L. Forming, Fracture and Corrosion Behaviour of Stainless Steel 202 Sheet Formed by Single Point Incremental Forming Process. *Mater. Res. Express* **2019**, *6*, 126540. [CrossRef]

26. Vigneshwaran, S.; Krishna, K.S.V.B.R.; Sekhar, K.C.; Sivaprasad, K.; Venkateswarlu, K.; Narayanasamy, R. A Study on the Work Hardening and the Effect of Triaxiality on the Fracture Behaviour of Some Cryorolled Aluminium Alloys. *Mater. Sci. Eng. A* **2016**, *678*, 165–177. [CrossRef]

27. Zaid, A.I.; Hememat, S. Investigation on the effect of titanium (Ti) addition to the Mg- AZ31 alloy in the as cast and after extrusion conditions on its metallurgical and mechanical characteristics. *Mater. Sci. Eng.* **2016**, *146*, 012026. [CrossRef]

28. Kim, Y.H.; Park, J.J. Effect of Process Parameters on Formability in Incremental Forming of Sheet Metal. *J. Mater. Process. Technol.* **2002**, *130*, 42–46. [CrossRef]